

See discussions, stats, and author profiles for this publication at: <https://www.researchgate.net/publication/24233379>

# Laser Tweezers Raman Spectroscopy Potential for Studies of Complex Dynamic Cellular Processes: Single Cell Bacterial Lysis

ARTICLE *in* ANALYTICAL CHEMISTRY · APRIL 2009

Impact Factor: 5.64 · DOI: 10.1021/ac8023476 · Source: PubMed

---

CITATIONS

20

READS

41

## 5 AUTHORS, INCLUDING:



De Chen

National Institutes of Health

18 PUBLICATIONS 409 CITATIONS

[SEE PROFILE](#)



Alexander Sabelnikov

East Carolina University

60 PUBLICATIONS 420 CITATIONS

[SEE PROFILE](#)

## Article

### Laser Tweezers Raman Spectroscopy Potential for Studies of Complex Dynamic Cellular Processes: Single Cell Bacterial Lysis

De Chen, L. Shelenkova, Y. Li, C. R. Kempf, and A. Sabelnikov

*Anal. Chem.*, 2009, 81 (9), 3227-3238 • DOI: 10.1021/ac8023476 • Publication Date (Web): 25 March 2009

Downloaded from <http://pubs.acs.org> on April 30, 2009

#### More About This Article

Additional resources and features associated with this article are available within the HTML version:

- Supporting Information
- Access to high resolution figures
- Links to articles and content related to this article
- Copyright permission to reproduce figures and/or text from this article

[View the Full Text HTML](#)



ACS Publications

High quality. High impact.

Analytical Chemistry is published by the American Chemical Society. 1155 Sixteenth Street N.W., Washington, DC 20036

## Articles

# Laser Tweezers Raman Spectroscopy Potential for Studies of Complex Dynamic Cellular Processes: Single Cell Bacterial Lysis

De Chen, L. Shelenkova, Y. Li, C. R. Kempf, and A. Sabelnikov\*

East Carolina University, Greenville, North Carolina 27858

The potential of laser tweezers Raman spectroscopy (LTRS) to study complex and dynamic cellular processes was investigated on the model of single *E. coli* cells lysed (1) from “outside” with egg white lysozyme and (2) from “within” by temperature-induced temperate bacteriophage  $\lambda$ cI857. The two lysis processes differed in the final outcome (incomplete vs complete cell lysis) as revealed by the dynamic laser light scattering and exhibited distinctive dynamic Raman spectra changes. The technique enabled for the first time at the cellular level to observe and quantify real time interaction of lysozyme with *E. coli* cells, “visualize” a side effect of the process due to the presence of EDTA, and correlate the process of cell wall disruption, as evidenced by the onset and development of asymmetric speckle scattering patterns, with release/escape of intracellular material (ribosomes, nucleic acids, proteins, etc.) quantified by the intensity changes of Raman signatures. Raman spectra changes observed during the lysis from “within” suggest alleged production of heat shock proteins are consistent with the occurring synthesis of phage-related proteins and are in good agreement with the calculated potential contribution of the above proteins to the Raman spectra. It was also established and validated that the contribution of cellular DNA to the Raman spectra of bacterial cells is negligible compared to RNA. The results open new venues for LTRS research and strongly suggest that LTRS has a great potential especially in investigation of real-time processes.

Recent progress in laser physics, quantum optics, and other fields of physics has given a new impetus for the development and application in biology of more rapid, more sensitive, and more informative spectral analytical methods based on mass, Raman, infrared, and other spectroscopies. Furthermore, some of these new methods have the capability to allow study of live, individual cells. Because the single-cell studies are not subject to the averaging effects of population-scale methods, they offer a new level of analysis unavailable with traditional biochemical methods.

Among these new techniques is confocal Raman microscopy,<sup>1</sup> in which the Raman signal from only the focal region of the objective is collected, while background signals that are out of the focus are rejected. This technique allows high spatial resolution and enables detection of both the spectral features of single cells and interior organelles. The main drawback of the method is that the targeted cell must be immobilized by physical or chemical contact. However, by combination of this approach with optical tweezers (single-beam optical trapping),<sup>2,3</sup> it becomes possible to analyze single, live, moving cells in aqueous solutions. This new combined technique, called confocal laser tweezers Raman spectroscopy (LTRS), has been used in studies of single, optically trapped microparticles, different prokaryotic and eukaryotic cells, and liposomal membranes.<sup>4–13</sup> Because the method is based on Raman signatures yielding information on covalent and hydrogen bonding, hydrophobic and electrostatic interactions, etc. in real time, it may be especially valuable for the elucidation of mechanisms of different dynamic processes occurring within cells. However, until now very few LTRS studies attempted to address cellular processes. Among them were a complex process of *Bacillus* sporulation<sup>10,11</sup> and an induced synthesis of recombinant proteins in bacterial cells.<sup>12,13</sup> In both cases, however, the evolution of particular Raman markers specific for the process (dipicolinic acid band for spores and markers associated with protein vibrations in the case of protein synthesis), has been followed. To further test and explore the analytical potential of LTRS, it would be interesting to employ more complex cellular processes with

- (1) Turrell, G.; Corset, J., Jr., Eds. *Raman Microscopy, Developments and Applications*; Academic Press: London, 1996.
- (2) Lankers, M.; Popp, J.; Kiefer, W. *Appl. Spectrosc.* 1994, 48, 1166–1168.
- (3) Sheetz, M. P. *Methods Cell Biol.* 1998, 55, xi–xii.
- (4) Ajito, K. *Appl. Spectrosc.* 1998, 52, 339–342.
- (5) Ajito, K.; Torimitsu, K. *Trends Anal. Chem.* 2001, 20, 255–262.
- (6) Xie, C.; Dinno, M. A.; Li, Y. Q. *Opt. Lett.* 2002, 27, 249–251.
- (7) Xie, C.; Li, Y. Q. *J. Appl. Phys.* 2003, 94, 6138–6142.
- (8) Chan, J. W.; Esposito, A. P.; Talley, C. E.; Hollars, C. W.; Lane, S. M.; Huser, T. *Anal. Chem.* 2004, 76, 599–603.
- (9) Xie, C.; Mace, J.; Dinno, M. A.; Tang, W.; Li, Y. Q.; Newton, R. J.; Gemperline, P. J. *Anal. Chem.* 2005, 77, 4390–4397.
- (10) Chen, D.; Huang, S. S.; Li, Y. Q. *Anal. Chem.* 2006, 78, 6936–6941.
- (11) Huang, S. S.; Chen, D.; Pelczar, P. L.; Veprachedu, V. R.; Setlow, P.; Li, Y. Q. *J. Bacteriol.* 2007, 189, 4681–4687.
- (12) Xie, C.; Nguyen, N.; Zhu, Y.; Li, Y. Q. *Anal. Chem.* 2007, 79, 9269–9275.
- (13) Chan, J. W.; Winhold, H.; Corzett, M. H.; Ulloa, J. M.; Cosman, M.; Balhorn, R.; Huser, T. *Cytometry, Part A* 2007, 71A, 468–474.

\* Corresponding author. Phone: 1-(252) 328-4983. Fax: 1-(252) 328-0753. E-mail: sabelnikova@ecu.edu.

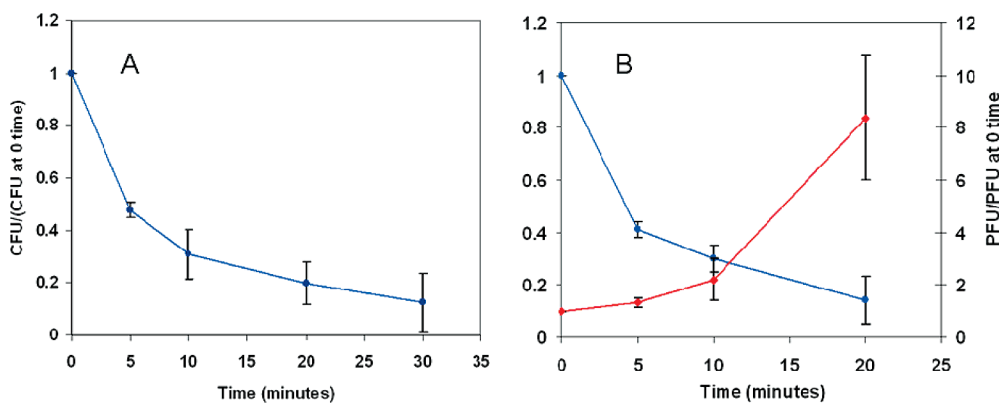


**Figure 1.** (A) lysis of *E. coli* K12 (HMS174) with lysozyme at 30 °C. Experimental points (colony forming units, CFU, normalized to CFU at 0 time) are presented as means  $\pm$  SE for 4 independent experiments; (B) lysis of lysogenic strain of *E. coli* K12 (HMS174/λcl857) by temperature induction of prophage at 45 °C. Left ordinate, normalized CFU (similar to part A); right, the normalized number of bacteriophage plaque forming units, PFU (red). Experimental points are presented as means  $\pm$  SE for at least three independent experiments.

fairly known molecular mechanisms. The latter could significantly help in interpretation, confirmation, and validation of the biological significance of observed Raman spectral changes (if any) at the cellular level. A good model of such cellular processes for LTRS analysis would be the process of bacterial cell lysis initiated by two different mechanisms: by exogenously added lysozyme and by induced temperate bacteriophage. There is a certain uniqueness of this biological model system for LTRS analysis in that it can be initiated by two different mechanisms, and LTRS can be tested to monitor the molecular differences

Lysozyme is a single chain protein with a MW of 14.3 kDa. It hydrolyzes  $\beta(1\text{-}4)$ -linkages between *N*-acetylmuramic acid (NAM) and *N*-acetyl-D-glucosamine (NAG) residues of peptidoglycan cell wall layers of all bacteria. It is an important, widespread lytic enzyme of the immune system.<sup>14,15</sup> In the 1960s and 70s, treatment of bacteria with lysozyme was widely used for the production of protoplasts or spheroplasts (cells devoid of cell walls but with functional cytoplasmic membranes) for early studies of genetic exchange and as one of the preparative tools for isolation of different bacterial cell components.<sup>16</sup> Lysis by lysozyme of a gram-negative bacterial cell, such as *E. coli*, is a decomposing enzymatic process that eventually brings about profound structural changes in the cell envelope, such as disruption of the rigid peptidoglycan layer that protects the cell against changes of osmotic pressure. As a result, osmotic collapse of the cytoplasmic membrane occurs and the cell dies.

Lysis by the induced prophage lambda is a more complex, programmed process that occurs in stages of different duration and is controlled by specific bacteriophage genes. Some of them direct the replication of phage DNA, production of capsid proteins, and assembly of new bacteriophage particles (for reviews see refs 17–19). Altogether, up to 100 new phage particles may be built and accumulated in one cell before its programmed lysis. The latter is controlled on a timely basis by several other specific genes. The precise mechanism of this timing is not yet completely understood.<sup>20–22</sup> Bacteriophage λ, similar to other double-stranded DNA phages, produces a soluble, muralytic enzyme known as an endolysin that is encoded by the *R* gene (for a review, see ref 20). For λ, the enzyme has a transglycosylase activity. It is turned on approximately 8 min into the vegetative cycle or after the induction of the prophage and is constitutively expressed thereafter. However, endolysins cannot permeate the cytoplasmic membrane

(CM), and in order to degrade the cell wall they require a “permeation factor”, a small membrane protein encoded by the *S* gene and called holin.<sup>21</sup> Synthesized holins are inserted into the CM and by a process of unspecific oligomerization gradually form tentative protein rafts/domains with reduced mechanical integrity. This may lead to local disruption of membrane integrity and depolarization, followed by the overall collapse of the transmembrane proton-motive force, quick and extensive permeabilization of the CM for endolysins, and the subsequent degradation of murein (peptidoglycan).<sup>23,24</sup> So holins, in fact, ultimately control the timing of lysis. In addition to *R* and *S* genes, many phages with Gram-negative hosts, including bacteriophage λ, have two other overlapping genes that encode the auxiliary lysis proteins *Rz* and *Rz1*. It is suggested that *Rz* and *Rz1* products form a complex having endopeptidase activity that cleaves the oligopeptide links between the murein and the outer membrane lipoprotein (Lpp).<sup>20</sup>

So, both lysis processes as reviewed above are accompanied by profound structural and molecular changes that take place primarily at the level of the cell envelope in a sequential fashion. However, the mechanisms, the nature, and temporal molecular patterns of these changes are likely to be different except for one feature, similar destructive enzymatic activity at the end of the lysis process. In contrast to the process of lysozyme lysis of the cell, phage-induced cell lysis involves additional, earlier events such as extensive protein (and nucleic acid) synthesis with concurrent insertion of synthesized holin molecules into the CM and their eventual aggregation, which may contribute to the overall kinetic picture of molecular/structural changes. So, both

- (14) Fleming, A. *Proc. R. Soc. London, Ser. B* **1922**, *93*, 306–317.
- (15) Blake, C. C.; Jonson, F.; Mairl, L. N. *Proc. R. Soc. London, Ser. B* **1967**, *167*, 378–388.
- (16) Haas, M. J.; Dowding, J. E. *Methods Enzymol.* **1975**, *43*, 611–628.
- (17) Friedman, D. I.; Court, D. L. *Curr. Opin. Microbiol.* **2001**, *4*, 204–207.
- (18) Gottesman, M. E.; Weisberg, R. A. *Microbiol. Mol. Biol. Rev.* **2004**, *68*, 796–813.
- (19) Oppenheim, A. B.; Kobiler, O.; Stavans, J.; Court, D. L.; Adhya, S. *Annu. Rev. Genet.* **2005**, *39*, 409–429.
- (20) Young, R.; Wang, I.; Roof, W. D. *Trends Microbiol.* **2000**, *8*, 120–128.
- (21) Wang, I.; Smith, D. L.; Young, R. *Annu. Rev. Microbiol.* **2000**, *51*, 799–825.
- (22) Ryan, G. L.; Rutenberg, A. D. *J. Bacteriol.* **2007**, *189*, 4749–4755.
- (23) Grundling, A.; Manson, M. D.; Young, R. *Proc. Natl. Acad. Sci. U.S.A.* **2001**, *98*, 9348–9352.
- (24) Wang, I.; Deaton, J.; Young, R. *J. Bacteriol.* **2003**, *185*, 779–787.

processes present a good model especially if compared for further elucidation of the analytical potential of real-time, single cell LTRS.

The results of the study presented below show the unique capabilities of LTRS for real-time analysis of complex biochemical processes within single live cells. LTRS can reliably identify Raman spectra patterns for both cases of single cell lysis studied and readily discriminate between them. Remarkably, this can be done even without the use of specific multivariate statistical analysis of the complex spectral data, which is often needed.<sup>11</sup> To our knowledge this is the first application of this emerging technique in a comparative study of complex cellular processes.

## EXPERIMENTAL SECTION

**Chemicals and Media.** LB (Luria broth) and PBS buffer were from Invitrogen (Carlsbad, CA), and egg white lysozyme was from Bio-Rad (Los Angeles, CA). All other reagents and chemicals (granulated agar, rifampin, EDTA, Tris-HCl, etc.) were from Thermo-Fisher Scientific (Waltham, MA).

**Escherichia coli Strains and Bacteriophages.** Different *E. coli* K12 strains, C600, HMS174 (F-*rec*A1, *rif*R, *Su*, rK12, mK12+) derivative of W3110 and KL16-99,<sup>25</sup> and HMS174 lysogenic for temperature inducible bacteriophage  $\lambda$ CI857 were used in this study. All strains were a generous gift of Dr. W. Studier (Brookhaven National Laboratory).

**Cell Growth.** Lysogenic (L) and nonlysogenic (NL) strains of *E. coli* were grown overnight in LB at 30 °C or 37 °C, respectively. The cells were seeded (1:6–10) in fresh LB and incubated with aeration (150 rpm) at the above temperatures until the optical density OD<sub>620</sub> = 0.4–0.5 was reached (~2–3 h, logarithmic phase of growth).

**Lysis with Lysozyme.** Exponentially grown *E. coli* K12 (HMS174) cells were spun down, washed with PBS, resuspended (final concentration, fc ~ 5 × 10<sup>6</sup> colony forming units (CFU)/mL) in 400 μL of lysing solution (4 μL of lysozyme from 3 mg/mL stock in distilled water kept at 4 °C, 1.5 mM EDTA, and 10 mM Tris-HCl, pH 7.0) and incubated at 30 °C for 30–60 min. Aliquots of the suspension were withdrawn at designated time points and after appropriate dilutions analyzed for the number of bacterial counts (CFU).

**Cell Lysis by the Temperature Induction of  $\lambda$  Prophage.** Exponentially grown lysogenic strain *E. coli* K12 (HMS174/( $\lambda$  CI857) was spun down, washed, and resuspended in fresh LB (fc ~ 5 × 10<sup>8</sup> CFU/mL). The suspension was incubated at 45 °C for about 20–30 min.<sup>26</sup> Aliquots of the suspension were withdrawn at designated time points and after appropriate dilutions analyzed for the number of bacterial counts, CFU, and released bacteriophage particles (plaque forming units, PFU).

**Laser Tweezers Raman Spectroscopy (LTRS).** The experimental setup of the LTRS was previously described in detail.<sup>11,27</sup> In short, a near-infrared (NIR, 785 nm) laser beam from a diode laser (TIGER, Sacher Lasetechnik, Germany), after circularization with a prism pair and collimation, was introduced into an inverted microscope (Nikon TE2000) equipped with a high numerical aperture objective (100×, NA 1.30). The laser beam was tightly

focused to form an optical trap. A bacterial cell in aqueous medium can be trapped ~10 μm above the bottom coverslip using the gradient force generated by the focused beam. The same laser beam excites Raman scattering from molecules inside the trapped cell. The collimated backward Raman scattering light, collected by the same objective, was focused onto the entrance slit of a spectrograph after spatial and spectral filtering and detected by a liquid nitrogen-cooled, charge-coupled detector (Symphony CCD, Jobin-Yvon). In this system, the image of the trapped cell can be viewed through a video camera illuminated with a green-filtered lamp. The Raman spectra of the trapped bacterial cell in the “fingerprint” range from 600 to 1800 cm<sup>-1</sup> were recorded with a spectral resolution of ~6 cm<sup>-1</sup>. The NIR diode laser was operated at 10 mW for a period of up to 1 h. Raman spectra were measured in a consecutive train of measurements, each with an acquisition time of 120 s. The microscope sample holder was made of a 3.8 mm thick brass slide into which a conical hole (6.6 mm (bottom) by 10 mm (top) in diameter) is drilled and sealed from the bottom with a glued quartz coverslip. This improvised cuvette could hold a sample of about 250 μL. It was mounted onto a laboratory-shop fabricated temperature controlled microscope stage equipped with a pair of Petri thermoelectric (TE) coolers and a temperature controller (TEC-2000, ThorLabs Inc., Newton, NJ). The temperature of the sample holder can be quickly increased from room temperature to a set temperature, e.g., ~50 °C in about 2 min and then maintained at the set temperature within accuracy of 0.2 °C. To reduce evaporation of samples during experiments, the cuvette was capped with a plastic lid.

The setup for the LTRS experiments with lysozyme was as follows. To freshly prepared lysis solution (250 μL), containing 2.5 μL of lysozyme (from 3 mg/mL stock in distilled water kept at 4 °C) in 1.5 mM EDTA and 10 mM Tris-HCl, pH 7.0, in the sample holder at 30 °C, 3–4 μL of *E. coli* cell suspension (of ~2 × 10<sup>5</sup>/mL) was added. (Lowering the temperature of incubation from 37 °C (optimal) to 30 °C was expected to prolong the process of lysis.) After about 1 min (time needed to capture a single *E. coli* cell in the laser trap), Raman spectra were collected continually until the changes were no longer observed (within less than an hour). In order to be certain that the observed changes were indeed due to the enzyme action, in each experiment Raman spectra of a control, a trapped cell in experimental solution but without lysozyme and EDTA, was measured under the same conditions for an hour.

The setup of the LTRS experiments with bacteriophage induced cell lysis was as follows. To freshly prepared solution (250 μL) of PBS-LB (2:1), pH = 7.4, in the cuvette maintained at 45 °C, 3–4 μL of *E. coli* (lysogenic for  $\lambda$  phage) cell suspension (of ~2 × 10<sup>5</sup>/mL) was added. Raman spectra were collected continually until the cell lysis (the cell disappears from the trap). LTRS measurements of cells of the nonlysogenic strain during 1 h at 45 °C were used as controls in these experiments.

In each LTRS experiment, the background spectrum (without the cell in the trap) was taken under the same acquisition conditions and subtracted from the spectra of individual cells. The subtracted spectra were then smoothed (3 or 5 points) using the Savitzky–Golay filter method. Each Raman spectrum reflected the chemical constituents of a particular cell trapped at random.

(25) Campbell, J. L.; Richardson, C. C.; Studier, F. W. *Proc. Natl. Acad. Sci. U.S.A.* **1978**, 75, 2276–2280.

(26) Lieb, M. *Science* **1964**, 145, 175–176.

(27) Xie, C.; Chen, D.; Li, Y. Q. *Opt. Lett.* **2005**, 30, 1800–1802.

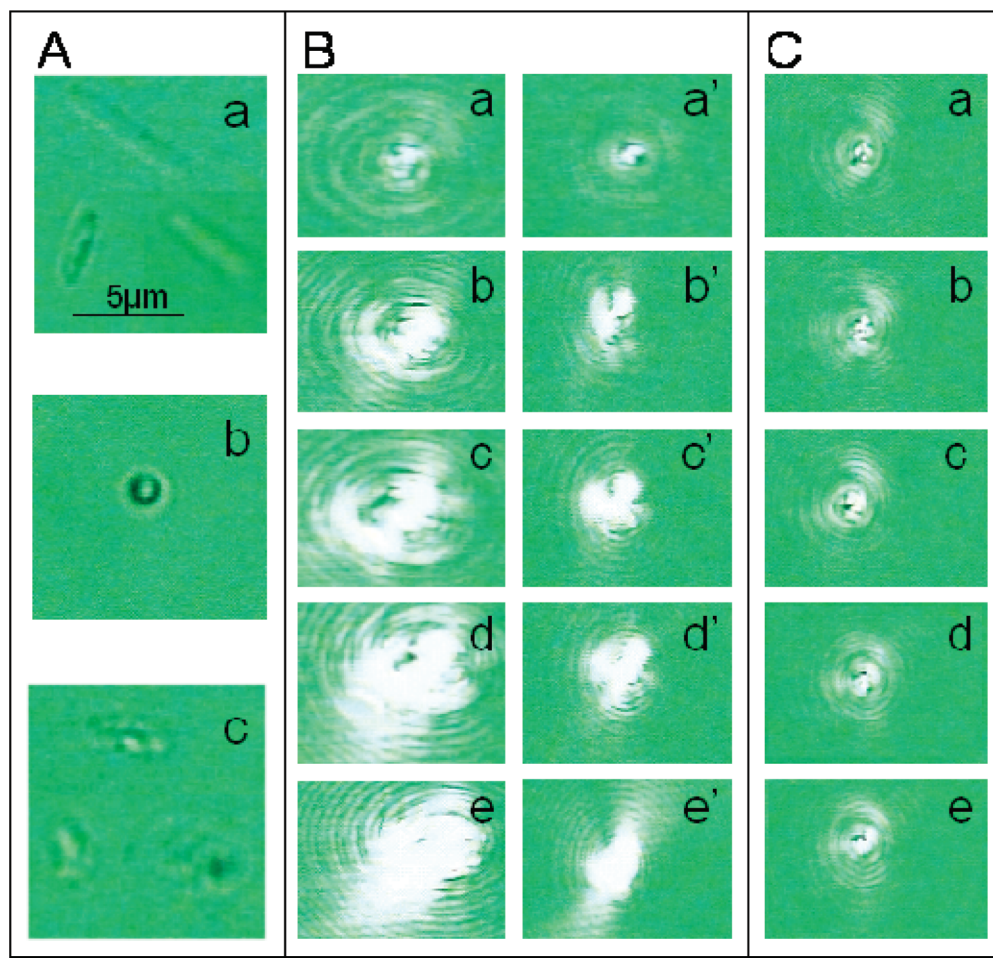


**Figure 2.** Real time images of cells during different lysis processes. (A(a and c)) images of cells in solution recorded with the NIR laser beam blocked and a BG-38 visible filter inserted before the camera; (A(b), B, and C) images of trapped cell recorded with the trapping NIR laser beam on and without the use of the BG-38; (A(a)) a typical *E. coli* cell in solution; (A(b)) trapped cell is always oriented perpendicular to the plane of image and is usually seen as a dark spherical particle with a very thin, bright "halo"; (A(c)) cell lysed with lysozyme in solution. (B) Kinetics of changes in light scattering (refractivity) of two representative cells being lysed by lysozyme, images a–e (2, 4, 6, 25, and 32 min) and iamges a'–e' (2, 5, 10, 25, and 36 min). (C) Kinetics of changes in light scattering (refractivity) of a cell being lysed by temperature induced bacteriophage  $\lambda$ .

Additional special control spectra were recorded for every experimental LTRS setup (see below).

**Data Processing.** The data for LTRS and CFU/PFU graphs were processed using Origin 6.0 (OriginLab, Corp. Northampton, MA) and Excel 2003 (Microsoft, Seattle, WA) software, respectively. Some graphs (CFU, PFU, and intensities of Raman bands vs time) were further normalized to their initial or maximal values. For instance, CFU and PFU were normalized to their values at 0 time; intensities of selected Raman bands in kinetic experiments were normalized to their maximal values (e.g., at 60 min on Figure 4A). Individual Raman band intensities were measured digitally as the difference between the peak and foot points of a particular band.

## RESULTS AND DISCUSSION

**Lysozyme and Phage Induced Lysis in Cell Populations.** Prior to LTRS studies we checked with conventional microbiological methods that both processes of cell lysis work properly in log phase cell populations under the conditions employed in the study. Therefore, the simplest protocol for the experiment was chosen (see the Experimental Section)

It is well-known that *E. coli* and some other Gram-negative bacteria are less susceptible to lysozyme (compared to Gram-

positive organisms) due to the presence of the outer membrane (OM), which constitutes a certain permeability barrier (especially to hydrophobic compounds), and a lower proportion of peptidoglycan.<sup>28,29</sup> Therefore, these cells are usually hydrolyzed in the presence of EDTA, high concentrations of Tris (around 200 mM), and mild cold osmotic shock, all of which destabilize the outer membrane and make it permeable to lysozyme.<sup>30,31</sup> However, to maximally reduce, or even abolish possible contributing effects of high concentrations of Tris and cold osmotic shock, the latter was omitted and a much lower concentration of Tris (10 mM) was used.<sup>32</sup> We found that *E. coli* K12 cells could still be lysed under these conditions at 30 °C. Figure 1A shows typical kinetics of cell viability changes during the treatment with lysozyme under the above conditions. The cells start to lose the ability to form colonies right from the time they are added to the lysing solutions, and by about the 30th minute of incubation, this ability is lost by the majority of cells.

- (28) Leive, L. *Ann. N.Y. Acad. Sci.* **1974**, 235, 109–129.
- (29) Lugtenberg, B.; Van Alphen, L. *Biochim. Biophys. Acta* **1983**, 737, 51–115.
- (30) Witholt, B.; Boekhout, M.; Brock, M.; Kingma, J.; Heerinkhuizen, H. V.; Leij, L. D. *Anal. Biochem.* **1976**, 74, 160–170.
- (31) Tsapis, A.; Kepes, A. *Biochim. Biophys. Acta* **1977**, 469, 1–12.
- (32) Leive, L.; Kollin, V. *Biochem. Biophys. Res. Commun.* **1967**, 28, 229–236.

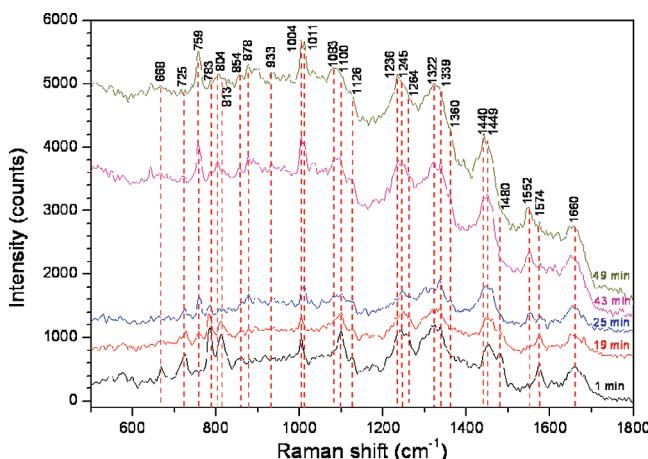


**Figure 3.** Real-time Raman spectra of a single *E. coli* cell during the lysis with lysozyme. Selective consecutive spectra are shown. Tentative assignments of the bands are presented in Table 1.

The loss of cell viability during the cell lysis induced by the phage is presented in Figure 1B. Therefore, both processes work properly on cell population under the conditions employed in this study. Importantly, the results of Figure 1A,B indicate that in both processes almost all cells ( $\sim 100\%$ ) are involved in the process and are affected, and therefore the problem of whether the “right”, representative cell is picked up for the LTRS analysis does not exist.<sup>33</sup>

**LTRS Experiments.** The current setup of the LTRS enabled both Raman spectral acquisition and bright field microscopic imaging simultaneously. Filtered visible green light illuminated the microscope viewing field which was displayed by a video camera system. It is worthwhile to note that because the process of cell lysis in both models develops over time, in each LTRS experiment only one representative cell might be randomly picked for investigation. This is why each LTRS experiment required fresh, exponentially grown cells (new batches). Apparently this factor could make an additional substantial contribution to the expected variability in the data to be obtained in different experiments.

**Laser Light Scattering.** On average, the concentration of cells used in the experiments provided about 4–5 moving cells per microscopic field ( $60 \mu\text{m} \times 100 \mu\text{m}$ ) per 20–30 s. So occasionally, the trapped cell under the investigation had to be moved to escape collision with another cell. Cell “crowding” had its advantages: the diminishing number of normal moving cells in the field surrounding a trapped cell provided additional evidence of cell lysis.

Images/frames of cells in solution were recorded with the NIR laser beam blocked and a BG-38 visible filter inserted before the camera to block the scattered IR light (Figure 2A,a,c). Images of trapped cell were recorded with the trapping NIR laser beam on and without the use of the BG-38 visible filter before the camera (Figure 2A,b; B and C). Therefore, the latter images were actually the backward speckle images of the NIR laser scattered from the trapped cell. The top image, a, in Figure 2A shows typical *E. coli* cells in solution. The trapped cell is always oriented perpendicular to the plane of image and is usually seen as a dark spherical

particle with a very thin, bright “halo” (Figure 2A,b). The cell lysed with lysozyme is seen as an irregular structure with blebs and protrusions of allegedly intracellular material (Figure 2A,c).

**Cell Lysis by Lysozyme.** During the process there is a significant change in the cell’s refractivity/light scattering. Kinetics of refractivity patterns of trapped *E. coli* cells during the lysis with lysozyme were monitored in time during 2 min intervals (the usual Raman spectra acquisition time used in current experiments). Several representative images in succession for two different cells, images a–e (2, 4, 6, 25, and 32 min) and iamges a’–e’ (2, 5, 10, 25, and 36 min) are shown in Figure 2B. They seem to reflect certain stages of the process. In the beginning of the process, the light scattering pattern (Figure 2B,a,a’) is symmetric and the scattering is weak. This may indicate the smooth surface of a still fairly intact cell in the laser trap. By 4–5 min, as the process progresses, the appearance of asymmetric speckle scattering patterns is observed. The rate of their development and their extent varied from cell to cell (total of six experimental cells) as evidenced by the images of Figure 2B. The results for panels a–e indicate that the asymmetric speckle scattering patterns are more powerful and still enhancing up until 25 min. In contrast, the panels a’–e’ exhibit “faster” and less extensive refractivity changes; no significant changes occur after 10 min. Noteworthy, in some especially motile cells, which upon LT entrapment exhibits rotation, the latter abruptly stops several minutes after the appearance of the first speckle scattering patterns which indicates the collapse of the proton motive force,  $\Delta\phi$ .<sup>23,34</sup> Though not quantitative, the appearance and development of asymmetric speckle scattering patterns indicate substantial changes of the cellular surface. Most likely, they reflect bulging out of the cytoplasmic membrane and some intracellular material through the enlarging gaps in the peptidoglycan layer known to be produced by the lysozyme action. Indeed, in separate experiments, turning the trapping NIR laser beam off when refractivity changes are no longer observed yielded an irregular structure with blebs and protrusions of intracellular material (Figure 2A,c). Importantly, the latter could be still held by the laser tweezers during the time of observation (1 h) which indicated that the cell was not completely disintegrated. In control experiments, where the lysozyme was absent from the solution, no visible changes of cells in LT traps were observed (one of them with EDTA is shown in Figure S-3, Supporting Information).

**Lysis by the Induced Bacteriophage.** The scattering image patterns of cells being lysed by the temperature induced bacteriophage  $\lambda$  (Figure 2C) were somewhat similar to the initial images of Figure 2B,a,a’. However, the bright speckle scattering patterns remain subdued and symmetrical until a sudden flash of light when the trapped cell abruptly vanished from the microscopic field. Apparently, changes within the cells accumulated until that moment became so dramatic that the cell burst into pieces which could no longer be held by the laser tweezers. In fact, after about 20–50 min, only very small amorphous objects possibly representing cell debris were seen in the microscopic field (not shown). This picture is consistent with the observation that “holins kill without warning”.<sup>23</sup> The time between the initiation of the process

(34) Mitchell, P. *Trans. Biochem. Soc.* **1976**, 4, 399–430.

(35) Tu, A. T. *Raman Spectroscopy in Biology: Principles and Applications*; John Wiley and Sons: New York, 1982.

(33) Sabelnikov, A.; Kempf, C. R. *Anal. Biochem.* **2008**, 383, 346–348.

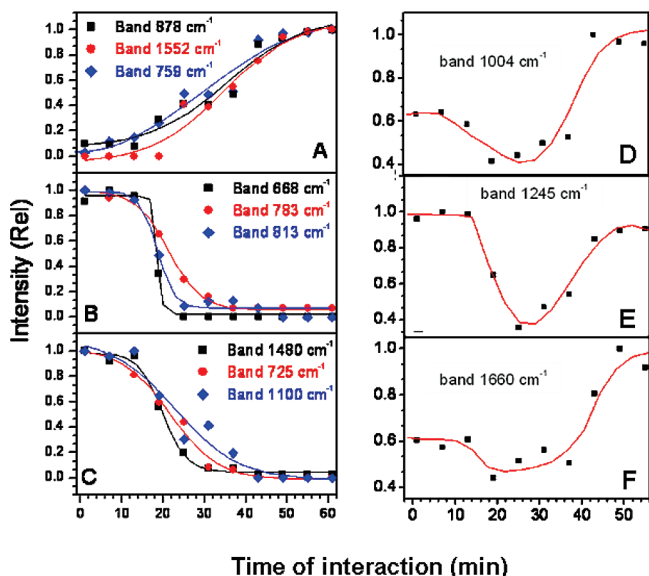


**Figure 4.** Kinetics of intensity changes of selective bands: (A) tryptophan assigned bands, (B and C) RNA assigned bands, (D) phenylalanine assigned band at  $1004\text{ cm}^{-1}$ , and (E and F)  $1245$  and  $1660\text{ cm}^{-1}$  bands (amide III and amide I bond vibrations, respectively).

and the final burst varied significantly between the cells, the average being  $35 \pm 13\text{ min}$  (mean  $\pm$  SD; 6 cells).

**Real-Time Raman Spectra.** Raman spectra of single cells acquired simultaneously with microscopic images during the cell lysis exhibited unexpected plethora of changes within the frequency range of  $660$ – $1700\text{ cm}^{-1}$ . Furthermore spectra change patterns were specific for each case of single cell lysis (compare columns 2 and 3 of Table 1).

**Spectra of Intact Live Bacterial Cells.** Typical spectrum of a single live bacterial cell of exponentially grown culture, exemplified by *E. coli*, is shown in Figure 3 (the first, bottom spectra). Evidently, the bands observed represent vibrational frequencies of molecular components, groups, assemblies, and interactions of almost all major constituents of the bacterial cell such as nucleic acids, proteins, lipids, and carbohydrates. However up until now, perhaps due to the very complex nature of Raman spectra of live cells and just a few publications on the subject, little consensus exists with regard to several major Raman bands of bacterial cells. For instance, one of the major bands of a cell spectrum at  $813\text{ cm}^{-1}$  is attributed to tyrosine (Y),<sup>7,13</sup> to lipids O–P–O,<sup>9</sup> or even DNA O–P–O<sup>–</sup> stretch,<sup>7</sup> though it is well-known that DNA in

the cell is in the B-form. Another one in the region of  $1090$ – $1100\text{ cm}^{-1}$  is assigned to carbohydrates<sup>44</sup> or “DNA/O–P–O<sup>–</sup>” at  $1099\text{ cm}^{-1}$ ,<sup>9</sup> or at  $1095\text{ cm}^{-1}$ ,<sup>13</sup> etc., the  $1449$ – $1451\text{ cm}^{-1}$  broadband is attributed to lipids,<sup>7,44</sup> protein and lipids,<sup>9,13</sup> or solely to proteins (ref 31 and references therein). Furthermore, nowhere in the literature devoted to Raman spectra of cells (both pro- and eukaryotic) could we find an estimate of the relative contribution of DNA and RNA to the spectra. Meanwhile, a paradigm prokaryotic cell (*E. coli*) contains about 7 times more RNA (21%) and 3 times more lipids (9.9%) than DNA (3.3%) by dry weight.<sup>45</sup> In addition, there are about 18 000 ribosomes/cell<sup>45</sup> in which RNA molecules retain highly ordered structure with the backbone conformation of the A-type helix characterized by a high intensity band at  $813\text{ cm}^{-1}$ .<sup>30,46</sup> So, we suggest that the nucleic acid related spectra observed are predominantly represented by RNA specific bands. The contribution of DNA is very small, and the Raman band at  $1092\text{ cm}^{-1}$  characteristic of the B-form of DNA<sup>37,38</sup> is masked by the expected significant symmetric stretching mode of RNA and the lipid phosphodioxy group ( $\text{PO}_2^-$ ) and the additional contribution of various single bond (C–C) stretching vibrations of the acyl chains of membrane phospholipids in the vicinity of this band.<sup>38</sup> A noticeable contribution of DNA in this region may be observed without RNA contribution and at higher DNA/lipid ratios, such as in the spectrum of DNA containing virions of bacteriophage PRD1 (DNA/lipid = 1).<sup>38</sup> It is also noteworthy that since the Raman scattering of nucleotides is substantially more intense than that of amino acid residues,<sup>47</sup> the interpretation of the spectra changes in regions where the contribution of both is expected should be very cautious.

**Spectra Changes during the Lysis with Lysozyme.** During the process of *E. coli* cell lysis by lysozyme, the Raman spectra changed significantly. A typical example of these changes is presented in Figure 3 (spectra above the first spectrum) and Table 1). The most dramatic changes took place in frequency ranges of  $650$ – $880$ ,  $1000$ – $1140$ ,  $1320$ – $1360$ ,  $1440$ – $1480$ , and  $1550$ – $1660\text{ cm}^{-1}$  (Table 1). Raman bands at  $668$ ,  $725$ ,  $783$ ,  $813$ ,  $1100$ ,  $1480$ , and  $1574\text{ cm}^{-1}$  decreased significantly in intensity or even disappeared completely. Others, such as bands at  $759$ ,  $878$ ,  $1011$ , and  $1552\text{ cm}^{-1}$  emerged and grew (Figure 3, spectra taken at different times, and Table 1). All these “changing” bands may be grouped into three clusters with regard to the time frame of their changes and the kinetics of changes relative to the observed onset and development of asymmetric speckle scattering patterns. (It should be noted that though the time frame and magnitude of the observed changes varied significantly from experiment to experiment (from cell to cell,  $n = 6$ ), the trends in the patterns and kinetics of changes remained fairly similar for all single cells studied (see Figure S-1 in the Supporting Information)).

**The First Group.** The first group contains the bands which emerge in the process and their intensity increases during the whole time of observation. Raman bands at  $759$ ,  $878$ ,  $1011$ , and

- (36) Benevides, J. M.; Tsuboi, M.; Bamford, J. K. H.; Thomas, G. J., Jr. *Biophys. J.* **1997**, 72, 2748–2762.
- (37) Thomas, G. J., Jr.; Benevides, J. M.; Overman, S. A.; Ueda, T.; Ushizawa, K.; Saitoh, M.; Tsuboi, M. *Biophys. J.* **1995**, 68, 1073–1088.
- (38) Tuma, R.; Bamford, J. H. K.; Bamford, D. H.; Thomas, G. J., Jr. *J. Mol. Biol.* **1996**, 257, 102–115.
- (39) Lippert, J. L.; Lindsay, R. M.; Schultz, R. *Biochim. Biophys. Acta* **1980**, 599, 32–41.
- (40) Tuma, R.; Prevelige, P. E., Jr.; Thomas, G. J., Jr. *Biochemistry* **1996**, 35, 4619–4627.
- (41) Aubrey, K. L.; Thomas, G. J., Jr. *Biophys. J.* **1991**, 60, 1337–1349.
- (42) Manoharan, R.; Ghiamati, E.; Britton, K. A.; Nelson, W. H.; Sperry, J. F. *Appl. Spectrosc.* **1991**, 45, 307–311.
- (43) Ataka, K.; Hegemann, P.; Heberle, J. *Biophys. J.* **2003**, 84, 466–474.
- (44) Schuster, K. C.; Urlaub, E.; Gapes, J. R. *J. Microbiol. Methods* **2000**, 42, 29–38.
- (45) Moat, A. G.; Foster, J. W. *Microbial Physiology*, 3rd ed.; Wiley-Liss, Inc.: New York, 1995.

- (46) King, T. C.; Rucinsky, T.; Schlessinger, D. *Nucleic Acid Res.* **1981**, 9, 647–661.
- (47) Thomas, G. J., Jr.; Prescott, B.; McDonald-Ordzie, P. E.; Hartman, K. A. *J. Mol. Biol.* **1976**, 102, 103–124.
- (48) Rupley, J. A.; Gates, V. *Proc. Natl. Acad. Sci. U.S.A.* **1967**, 57, 496–510.
- (49) Phillips, D. C. *Proc. Natl. Acad. Sci. U.S.A.* **1967**, 57, 484–495.

**Table 1. Raman Bands Observed during Cell Lysis by Lysozyme and by Temperate Phage, Their Changes, and Tentative Assignment<sup>a</sup>**

band ( $\text{cm}^{-1}$ )	lysozyme	bacteriophage	tentative assignment	ref
668	↓		ring breathing (G)	36
725	↓		ring breathing (A)	36, 37
759	↑	absent	Trp (W); $\nu(\text{C}-\text{N}^+)$ lipids; T	38
783	↓	no change	$\nu(\text{O}-\text{P}-\text{O})$ lipids	39
805	↑		ring breathing (C,U)	36
813	↓	↓	$\nu(\text{O}-\text{P}-\text{O})$ lipids	39
854	↑↓	↓	$\nu(\text{O}-\text{P}-\text{O})$ RNA	36
878	↑	absent	Tyr (Y); $\nu(\text{O}-\text{P}-\text{O})$ lipids	38, 41
933	↑		Trp (W); acyl $\nu(\text{C}_1-\text{C}_2)$	38
1004	↑↓	↑↓	sc $\nu(\text{C}-\text{C}_\alpha)$ , memb prot	38
1011	↑	absent	Phe (F)	38, 40
1032		↑	Trp (W)	39, 41, 42
1083	↑		Phe (F)	38, 40
1091–1094			prot: $\delta(\text{C}-\text{O})$ , $\delta(\text{CH}_3)$ .	40
1100	↓ (?)	no change	acyl in <i>gauche</i>	38
1126	↑↓	↑	Sym $\nu(\text{O}-\text{P}-\text{O}^-)$ DNA/lipids	37, 38
1245	↑↓		sym $\nu(\text{O}-\text{P}-\text{O}^-)$ RNA	36
1319		←	prot: sc $\nu(\text{C}-\text{C})$	40
1322	↑		acyl in <i>trans</i>	38
1339		↓	Am III[ $\beta$ -strand]	38
1360	↑		Am III	38, 40
1440	↑	↑	Am III in egg white lys	39
1447	↑		Nucleic acids (A, G)	37, 38
1480	↓		sc $\delta(\text{CH}_2)$ ; Trp (W)	38
1552	↑	absent	Trp (W)	38, 39
1574	↓		acyl $\delta(\text{CH}_2)$ , $\delta(\text{CH}_3)$	38
1584		↑	prot: sc $\delta(\text{CH}_2)$	38, 40
1617		↑ (?)	ring mode (G, A)	36, 37
1660	← (?) ↑		Trp (W); P ( $\text{C}_{5a}=\text{N}_5$ )	38, 43
1665		↑↓	ring mode (A,G)	36, 37
			Phe (F)	38, 40
			Tyr(Y)	38, 40
			Am I in lysozyme	39
			Am I (strand)	38, 40

<sup>a</sup> Primary information for almost all bands was taken from the 1982 textbook of A. T. Tu.<sup>35</sup> The ref column contains relevant later references. Abbreviations: Am, amid; acyl, acyl chains of lipids; prot, protein;  $\nu$ , stretching vibration of a specific group in parenthesis;  $\delta$ , deformation of a specific group in parenthesis; sc, nonaromatic side chain; sym, symmetrical; Trp, tryptophan; Phe, phenylalanine; Tyr, tyrosine; A, adenine; G, guanine; C, cytosine; T, thymine; U, uracil.

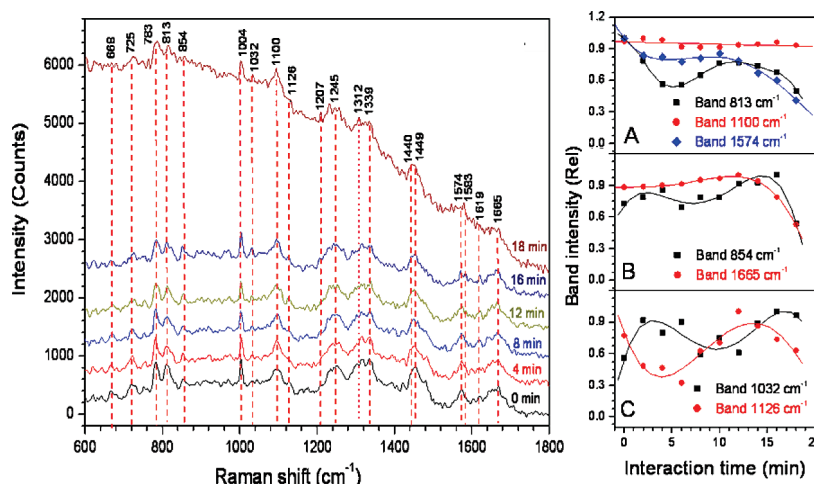


**Figure 5.** A representative example of real time Raman spectra of *E. coli* cell lysis by lysogenic, temperature-inducible bacteriophage ( $\lambda$ cI857) at 45 °C. Left panel, selective consecutive spectra taken at different times of bacteriophage induction are shown. Tentative assignments of the bands are presented in Table 1. Right panel, representative examples of kinetics of intensity changes of selective bands during the process: (A) RNA-related bands, (B) tyrosine assigned band at 854  $\text{cm}^{-1}$  and amide I band at 1665  $\text{cm}^{-1}$  (strand), (C) phenylalanine assigned band at 1032 and 1126  $\text{cm}^{-1}$  band tentatively assigned to the nonaromatic side chain vibrations of ribosomal proteins.

1552  $\text{cm}^{-1}$  represent this group. The time dependence of the band intensity changes for some of these bands shown in

Figure 4A exhibits sigmoidlike kinetics: slow beginning, faster phase, and leveling off. Interestingly, the beginning of the faster

**Table 2. Theoretically Calculated Amounts of Acidic Phospholipids (Phosphatidylglycerol, PG, and Cardiolipin, CL) in Outer (OM) and Cytoplasmic Membranes (CM) of *E. coli*, and the Maximal Amounts of Bound Lysozyme<sup>a</sup>**

<i>E. coli</i> membranes	membrane surface occupied by PG/CL (nm <sup>2</sup> × 10 <sup>5</sup> )	PG/CL (moles × 10 <sup>5</sup> )	maximum quantity of lysozyme (moles × 10 <sup>5</sup> )
external layer of OM, after EDTA	4.3	6.7	0.32
OM + CM	31.2	48	2.4

<sup>a</sup> In calculations the following numbers were used:  $2.8 \times 10^{-14}$  g of lipids per average *E. coli* cell;<sup>40</sup> 700, as an average mol mass of a phospholipid; the cell contains mainly PE, PG, and CL. They are distributed between three layers: one inner layer of OM and two layers of CM;<sup>29</sup> PE–PG/CL % ratio for OM is 9:1; for CM, 70:30;<sup>29</sup>  $1.26 \times 10^7$  nm<sup>2</sup> for a total surface of an average *E. coli* cell (a rod with  $L = 3 \mu\text{m}$  and  $D = 1 \mu\text{m}$ ) is  $0.64 \text{ nm}^2$  (ref 56) and  $\sim 13.5 \text{ nm}^2$  (ref 53) were taken as the average molecular area per phospholipid headgroup and lysozyme molecule cross-section, respectively. See the text for more details.

phase coincides with the observed onset and development of asymmetric speckle scattering patterns. All the bands exhibiting the above kinetics of their intensities may be assigned to normal modes of tryptophan (W) and most likely reflect the interaction of lysozyme with the cell. In fact, 759, 1004, 1011, and 1552 cm<sup>-1</sup> bands are all very strong tryptophan bands of lysozyme in aqueous solution.<sup>48</sup> Further, the lysozyme molecule contains six tryptophan residues, and two of them, Trp-62 and Trp-63, may form hydrogen bonds between NH groups of their side chains and O(6) and O(3) atoms of *N*-acetylglucosamine molecules during murein hydrolysis<sup>49</sup> later in the process. Also there are two other emerging Raman bands at 1360 and 1322 cm<sup>-1</sup>. The first may be assigned to a tryptophan mode which is very sensitive to the local environment around the residue.<sup>38,39</sup> Its intensity also exhibits sigmoidlike kinetics (Figure S-2C in the Supporting Information). The second is a characteristic Amid III band of lysozyme in aqueous solutions.<sup>39</sup> So, taken together all these data strongly suggest that all of these bands can be ascribed to lysozyme. Then the observed sigmoid-shaped kinetics of binding may represent two different stages of the process. The first, slow phase may reflect the initial binding of the enzyme to the cell and the time needed by the enzyme to provide enough breaks in the peptidoglycan for the visual cell envelope changes. The second, faster stage, which coincides with the onset and development of asymmetric speckle scattering patterns and seems to extend further, may reflect the additional binding/interaction of the lysozyme with membrane remnants of the disrupted cell. In this respect it is interesting to theoretically estimate the amount of lysozyme which can bind to the cell. The results of this estimation are presented in Table 2. It is well-known that the lysozyme as a basic protein with an isoelectric point of 11.0 binds strongly to acidic phospholipids, such as phosphatidylglycerol (PG), cardiolipin (CL), phosphatidylserin (PS), etc.<sup>39,50–53</sup> On the

other hand, the outer membrane (OM) of an intact *E. coli* K12 cell does not contain any phospholipids in the external layer, the latter being represented by lipopolysaccharide molecules, LPS ( $\sim 68\%$  of the cell surface), and the main OM proteins, such as Omp C, F, A, etc. ( $\sim 32\%$  of the surface).<sup>29</sup> However, treatment of the cells with EDTA in the presence of Tris releases up to 50% of the LPS molecules.<sup>28,32</sup> Its place in the external layer is immediately occupied by the phospholipids of the internal layer or even of the cytoplasmic membrane, CM.<sup>29</sup> The internal layer is represented by phosphatidylethanolamine (PE) and PG in the average ratio of 9:1. Taken together all these data indicate that at the initial stage of the interaction of the cell with lysozyme only about 3.4% of the external layer of the OM is occupied by the acidic phospholipids. So, at the initial, slow stage process (see Figure 4A), the maximal number of lysozyme molecules which can bind to OM is about  $3.2 \times 10^4$  (Table 2). At the faster stage, more acidic phospholipids partly from the inner layer of the OM and mainly from bulging CM (with much higher content of PG/CL, up to 30%)<sup>29</sup> become available for lysozyme binding (Table 2). Interestingly, the maximal estimated amounts of the bound enzyme at this stage (Table 2, the last column) exceeds the initial levels by a factor of 7.5, which is in excellent agreement with the results of Figure 4A.

**The Second Group.** The second group is represented by bands at 668, 725, 783, 813, 1100, 1480, and 1574 cm<sup>-1</sup> with an intensity decrease occurring simultaneously with the appearance and development of asymmetric speckle scattering patterns (Figure 4B,C). All these bands may be assigned to nucleic acids (different bases, their bonding, O–P–O and PO<sub>2</sub><sup>-</sup> stretches, etc. (Table 1) and, as we suggested above, are predominantly RNA related bands. Straightforward interpretation of these results might be the leak/escape of RNA-related material (ribosomes, ribosome subunits, r-RNA, m-RNA, t-RNA) from the cell ripped open by lysozyme. However, it is well-known that prolonged EDTA treatment of cells suspended in rather high concentrations of Tris (0.12 M) significantly affects cell viability which is accompanied by the destruction of cellular RNA and increased cell permeability.<sup>28,32,54</sup> It is also known that EDTA (a well-known chelating agent) disrupts the integrity of ribosomes which is highly dependent on Mg<sup>2+</sup>. Furthermore, King and coauthors<sup>46</sup> showed on isolated *E. coli* ribosomes that after a 5 min exposure to 10 mM EDTA at 25 °C none of the ribosomes retained their native structure and the 813 cm<sup>-1</sup> band (characteristic for in chain phosphodiester (O–P–O) symmetric stretch of dsRNA) was greatly diminished. Thomas and coauthors<sup>55</sup> however, using apparently lower concentrations of EDTA, came to the opposite conclusion that little if any conformational changes occur in rRNA upon the dissociation of 70S ribosomes into subunits.

(54) Neu, H. C.; Ashman, D. F.; Price, T. D. *J. Bacteriol.* **1967**, *93*, 1360–1368.

(55) Thomas, G. J., Jr.; Prescott, B.; Hamilton, M. G. *Biochemistry* **1980**, *19*, 3604–3613.

(56) Gulik-Krzywicki, T.; Shechter, E.; Vittorio, L.; Faure, M. *Nature* **1969**, *223*, 1116–1121.

(57) Pitout, M. J.; Conradie, J. D.; Van Rensburg, A. J. *J. Gen. Virol.* **1969**, *4*, 577–583.

(58) Arsene, F.; Tomoyasu, T.; Bukau, B. *Int. J. Food. Microbiol.* **2000**, *55*, 3–9.

(59) Casjens, S. R.; Hendrix, R. W. *J. Mol. Biol.* **1974**, *88*, 535–545.

In our experiments we intentionally used much lower concentrations of Tris (10 times less than those of refs 28 and 32) and EDTA (1.5 mM vs 10 mM).<sup>46</sup> Nevertheless, EDTA alone, in the absence of lysozyme, did bring about a reduction of the intensity of the 813 cm<sup>-1</sup> band although only a fraction (28%) of the changes observed in experiments with lysozyme. (Two representative spectra, at the beginning (4 min) and at the end (24 min) of the changes in the 813 cm<sup>-1</sup> band intensity are presented in Figure S-3 in the Supporting Information.) A lack of changes in light scattering patterns (Figure S-3 in the Supporting Information, image inserts) suggests that no substantial permeability changes occur in this case. The latter is further supported by the lack of intensity changes of most other RNA-related bands (see Figure S-3 in the Supporting Information and Table 1). Consequently, it is most likely that in the presence of EDTA alone, the diminishing intensity of the 813 cm<sup>-1</sup> band does reflect partial loss of the A-helix structure of rRNA upon unfolding of ribosomes within the cell interior. This suggestion may be further supported by the observed decrease (Figure S-3, Supporting Information and difference spectra) of the intensity of some protein related bands at 936 (bond stretching vibrations in proteins), 974, and 1126 cm<sup>-1</sup> (nonaromatic side chain vibrations),<sup>38,40</sup> which we tentatively assign to ribosomal proteins. It seems that a decrease of the number of rRNA nucleotide residues in the 3'-endo conformation (813 cm<sup>-1</sup> band) occurs without changing in base stacking, since we do not observe any intensity changes of other RNA-related bands (Figure S-3, Supporting Information). Unfolding may eventually result in extensive degradation of the unfolded particles by activated ribonuclease.<sup>46</sup>

So, the results with EDTA (Figure S-3 in the Supporting Information) suggest that during the process of cell lysis by lysozyme, the unfolding of part of the ribosomes and partial loss of secondary structure of rRNA may occur prior to the extensive rupture of the cell membranes. The massive release of the unfolded and degraded ribosomes, proteins, fragments of RNA, and pools of nucleotides from the cell will then follow upon the collapse of the membranes. We suggest that the 813 cm<sup>-1</sup> band may be used as a marker during the lysis by lysozyme in determining the time when the cell may be considered "lysed": when its intensity changes are no longer observed. Thus defined, this time will be 18 ± 5 min (m ± SD, 6 cells).

**The Third Group.** The third group of bands includes the bands the intensity of which first decreases simultaneously with the appearance and the development of asymmetric speckle scattering patterns and then increases to levels even higher than the initial values. Several Raman bands may be considered for this group: 1004 cm<sup>-1</sup> phenylalanine (F) mode, 1339 cm<sup>-1</sup> (Trp/A,G), 1449 cm<sup>-1</sup> (deformation of CH<sub>2</sub> groups in proteins), 1245 and 1660 cm<sup>-1</sup> (amide III and amide I bond vibrations, respectively) (Figures 3 and 4D–F and Figure S-2A,B in the Supporting Information). The most reasonable explanation for the initial decrease in band intensities is to suggest the loss of periplasmic and intracellular protein, amino acid, and nucleotide pools due to the extensive disruption of

the cell. The comparison of the results presented in Figure 4 (panel A vs B–F) suggests that the loss should be enormous, since it is not completely masked by the amounts of lysozyme still in the process of binding to the cell (panel A). The subsequent increase of the intensity of the bands at the later stage of the process (panels D–F) when the efflux of intracellular components stopped, may suggest that it is now due to the lysozyme molecules which continue binding to the acidic phospholipids of the remnants of the cellular membranes (panel A). Indeed, 1004 and 1660 cm<sup>-1</sup> bands are among the major bands in the spectrum of lysozyme in aqueous solutions.<sup>39</sup> With regard to 1245 cm<sup>-1</sup> band, it is worthy to note that lysozyme in aqueous solutions has three overlapping bands in the amide III region at 1257, 1240, and 1267 cm<sup>-1</sup>,<sup>39</sup> which may be seen in the top two spectra of Figure 3 at 1255, 1236, and 1264 cm<sup>-1</sup>. So, at this stage of the interaction process (see Figure 3, top two spectra), the intensity at 1245 cm<sup>-1</sup> apparently represents the superposition of the intensities of the above three bands of the enzyme.

**Bands Which May Be Specifically Associated with the Lysozyme/Membrane Lipids Interaction.** Changes in several bands, assigned to the lysozyme and membrane phospholipids, may provide some information about the nature of the final product of the lysis (an irregular structure with blebs and protrusions of intracellular material (Figure 2A,c)) and its interaction with lysozyme. Changes in conformationally informative lysozyme amide III bands at 1236 ( $\beta$ -sheet), 1257 (random coil), and 1264 cm<sup>-1</sup> ( $\alpha$ -helix) (Figure 3, the two top spectra) might indicate a preferential conformation of the enzyme during its interaction with the acidic phospholipids.<sup>39</sup> However, we failed to detect significant shifts in intensity of both Raman amide III bands (1236 and 1264 cm<sup>-1</sup>) and Raman amide I band at 1660 cm<sup>-1</sup> (assigned to  $\alpha$ -helix of lysozyme).<sup>39</sup> The evidence of a significant intensity increase of the other two bands characteristic of the  $\alpha$ -helix, amide III band of lysozyme at 1322<sup>39</sup> and 933 cm<sup>-1</sup> assigned to protein skeletal C–C and C–N vibrations<sup>40</sup> (Figure 3, the two top spectra) is also inconclusive, since the results may just indicate additional binding of the enzyme to the cell membrane remnants.

Among the bands which may be assigned to membrane phospholipids is the band at 804 cm<sup>-1</sup>. Significant increase of its intensity is observed at the later stages of the process (Figure 3). Lippert and coauthors<sup>39</sup> have also observed intense bands at 782 and 804 cm<sup>-1</sup> during the interaction of lysozyme with phosphatidylcholin/phosphatidic acid liposomes which they assigned to the O–P–O diester stretching mode of lipids. So, changes in the intensity of the 804 cm<sup>-1</sup> band in our case may be attributed to the electrostatic interaction of lysozyme with negatively charged phosphate head groups of PG and CL. Further, it is well-known from the studies of model (mostly liposome) systems (reviewed in refs 51 and 52) that lysozyme shows both polar and nonpolar binding with acidic lipids: electrostatic binding followed by hydrophobic associations. The hydrophobic contacts between the protein and lipid occur at the interface, resulting in an increase in the area per phospholipid molecule, deformation in the acyl chain packing, an increased fluidity of membrane, thinning of the bilayer, and increased membrane permeability.<sup>51,52,56</sup> Indeed,

at a later stage of the process of cell lysis with lysozyme we observe profound changes in the broad envelope of Raman bands in the interval of 1060–1150 cm<sup>-1</sup> and at 1440 cm<sup>-1</sup> (Figure 3), which may be interpreted in terms of the above phenomena. The increase of the intensity of the broad peak at around 1083 cm<sup>-1</sup> (Figure S-4 in the Supporting Information) may be due to the enhancement of the symmetric stretching mode of the lipid phosphodioxy group, PO<sup>-2</sup>, which is expected near 1092 cm<sup>-1</sup> (ref 31) and/or to the increase of membrane fluidity. The 1082 cm<sup>-1</sup> band is known as a characteristic mode for the liquid phase with acyl chains in the *gauche* conformation (ref 38 and references therein). The 1440 cm<sup>-1</sup> band assigned to deformation of acyl side-chains (bending vibrations of methyl and methylene groups)<sup>38</sup> gets more prominent with time (Figure 3) and may reflect the hydrophobic interaction of membrane lipids with lysozyme.

**Raman Spectra Changes during the Lysis by Induced Bacteriophage.** In contrast to the Raman spectra results presented above, only moderate changes in the Raman spectra were observed during the process of lysis by the induced bacteriophage (Table 1). A representative example of Raman spectra changes observed is shown in Figure 5 (left panel). It should be noted that similar to the experiments with lysozyme, there was a variability among the single cells studied ( $n = 6$ ) both in the time of the lysis process (see the section on laser scattering) and the intensity of certain Raman bands. However, again like with lysozyme experiments, the same pattern of changes was observed in all cells. Comparison of the data presented in Table 1 and the Raman spectra in Figures 5 (left panel) and 3 reveal significant differences between the two processes.

**Bands Assigned to Nucleic Acid Vibrations.** All bands assigned to nucleic acid vibrations, and particularly to RNA (left panel and right panel A of Figure 5), exhibit a completely different pattern of changes compared to those in Figures 3 and 4B,C. It should be noted that in spite of the fact that additional DNA is produced during the process without degradation of the host DNA, DNA-related bands will still remain masked by the dominating moieties of RNA, protein, and lipid. Simple calculation shows that even with the maximum contribution of newly synthesized phage DNA (if to assume the maximal phage burst size of 100 virions/cell and the amount of DNA per virion of  $4.75 \times 10^{-17}$  g),<sup>57</sup> the ratios of RNA/DNA, protein/DNA, and lipid/DNA will be 4, 12, and 2, respectively.

There is an initial decrease in the intensity of the bands at 813 and 1574 cm<sup>-1</sup> (right panel A in Figure 5) and some other nucleic acid related bands (not shown), except for the 783 and 1100 cm<sup>-1</sup> bands. Controls (isogenic *E. coli* strain without a temperate bacteriophage at 45 °C) in the case of 813 and 1574 cm<sup>-1</sup> kinetics exhibit a monotonous shallow decrease in time with no peaks and plateaus (not shown). We suggest that the decrease is due to a partial unfolding of ribosomes and partial loss of the double-stranded structure of ribosomal and possibly other RNAs at 45 °C. Two observations argue in support of this suggestion. The first is the lack of intensity changes of the 783 (not shown) and 1100 cm<sup>-1</sup> bands (right panel A of Figure 5), which do not depend on RNA conformation.<sup>46,47</sup> The other is that the intensity changes of

the 1126 cm<sup>-1</sup> band which we earlier tentatively assigned to nonaromatic side chain vibrations of ribosomal proteins (Figure S-3 in the Supporting Information) closely follow the kinetic profile of the 813 cm<sup>-1</sup> band of rRNA (right panel C of Figure 5). The initial decrease of the intensities of the 813 and 1574 cm<sup>-1</sup> bands gives way to a bell-like increase later in the process, which may suggest an increase in the number of ribosomes (dsRNA) for the subsequent phage-related DNA and protein synthesis.

**Protein-Associated Bands.** In contrast to the process of lysis by lysozyme, during the phage-induced lysis, bands at 759, 878, 1011, and 1552 cm<sup>-1</sup> assigned to tryptophan are either completely absent or hardly detectable. (In fact, this may be regarded as additional evidence in favor of the assignment of these bands to lysozyme tryptophan in the experiments above.) Bands assigned to phenylalanine and tyrosine, such as 854 (Y), 1004 (F), 1032 (F), 1207 (F,Y), and 1585 cm<sup>-1</sup>(F,W), are readily observable and seem to exhibit different and complex kinetics (representative spectra in the left panel of Figure 5). Furthermore, several other protein-related bands, such as amide III and I bands at 1319 (α-helix) and 1665 cm<sup>-1</sup>(strand), respectively, and the 1126 cm<sup>-1</sup> band (tentatively assigned to nonaromatic side chain vibrations of ribosomal proteins (Figure S-3 in the Supporting Information)) also exhibit noticeable changes during the process.

Representative examples of time dependence of the intensity changes for some of the bands are presented in the right panels B and C of Figure 5. In control experiments (isogenic *E. coli* strain without temperate bacteriophage at 45 °C), much simpler changes of protein related bands were detected during the time of observation (exemplified by Figure S-5 in the Supporting Information). The kinetic curves for aromatic vibrations, Y and F, seem to suggest two “humps”: one earlier and the second later in the process. The timing and nature of the second hump are consistent with the production of mature bacteriophage particles, which is observed under the same conditions in population-scale experiments (Figure 1B).

The first hump might reflect an early synthesis of heat shock proteins (HSPs) known to be produced by *E. coli* in response to a temperature upshift from 30° to higher temperatures ( $\geq 42$  °C). The response is positively controlled at the transcriptional level by the product of the *rpoH* gene, the heat shock promoter-specific  $\sigma^{32}$  subunit of RNA polymerase. At steady-state conditions, the region of *rpoH* mRNA containing the initiation codon and Shine–Dalgarno sequence forms a double-stranded structure which prevents its translation. At the increased temperature, partial melting of the mRNA secondary structure enables the ribosome binding, translation, and the subsequent production of HSPs (for a review, see ref 58). This partial melting of the *rpoH* mRNA might contribute to the initial decrease of the intensity of the 813 cm<sup>-1</sup> band (Figure 5A) which we earlier assigned to the partial loss of RNA secondary structure. Furthermore, there is also an early slight intensity increase of the 854 cm<sup>-1</sup> band in control experiments (Figure S-5 in the Supporting Information). The latter, however, might have been expected to be much stronger, if HSPs had been synthesized to the full extent of 15–20% of total cell protein at 46 °C.<sup>58</sup>

For further validation and better interpretation of these results, we estimated the amounts of all the main proteins synthesized ( $\lambda$ -related), or allegedly synthesized (HSPs) during the process, their aromatic residues content, and potential contribution to the initial Raman spectra (Table S-1 in the Supporting Information). Comparison of these data with those for lysozyme and myelin oligodendrocyte glycoprotein (MOG (1-120)) calculated from the results of Chan and coauthors,<sup>13</sup> which are also included in Table S-1 in the Supporting Information indicates several interesting issues. First, the preponderance of phenylalanine and tyrosine residues in HSPs and  $\lambda$  related proteins is consistent with the observed dominance of phenylalanine (F) and tyrosine (Y)-related bands in Raman spectra changes observed (Table 1 and Figure 5). Second, inconsistency between the expected amounts of HSPs and the small LTRS response suggests that only small amounts of these proteins are synthesized during temperature induced bacteriophage cell lysis. Since the synthesis (if any) of HSPs under the conditions of phage-induced cell lysis was not among the goals of the present paper, we did not pursue this question further. Third, the total amount of  $\lambda$ -related proteins (by weight and by aromatic residue contents) is comparable to the amounts of proteins that have been detected in case of lysozyme experiments (above) and during the expression of foreign protein MOG (1-120) in *E. coli* cells.<sup>13</sup> This indicates the validity of the detection of protein-related changes by LTRS during phage induced lysis and also suggests a rough general detection limit for proteins by LTRS without the use of a specific multivariate statistical analysis of the complex spectral data: around 3% of the cell total amount of protein ( $4.75/154 = 3.08\%$ , see Table S-1 in the Supporting Information). Fourth, though up to  $1-5 \times 10^3$  holin proteins (mol mass 11.13 kDa) may be present in the membrane at the time of triggering spontaneous lysis later in the process,<sup>20,21</sup> their direct contribution to the initial protein associated Raman scattering patterns is negligible compared to the virion proteins. So, the second “hump” of the kinetic curves for 854 (Y),  $1032\text{ cm}^{-1}$  (F), and the kinetic curve for amide I band at  $1665\text{ cm}^{-1}$  (strand) most likely reflect the changes associated with the synthesis and assembly of  $\lambda$  virion proteins (right panel B and C of Figure 5).

One particular point with regard to holin molecules deserves further discussion. In contrast to  $\lambda$  virion proteins which accumulate in the cytoplasm and most likely assemble into mature phage particles at the inner surface of the CM, holins accumulate inside the CM.<sup>20-24</sup> Particularly this event finally causes saltatory and generalized membrane disruption and cell lysis. However, as judged by the maintenance of  $\Delta\mu_{\text{H}^+}$  (proton motive force) up until the very last moment when the abrupt changes in membrane permeability occur, holins create their lethal membrane lesion without causing prior degradation of CM integrity.<sup>23</sup> On the other hand, holin has a positively charged C-terminal domain and two or three  $\alpha$ -helical transmembrane domains.<sup>21</sup> So, it is reasonable to assume that its electrostatic and hydrophobic interaction with acidic phospholipids (PG/CL) of the CM can be detected by the changes in lipid-associated Raman scattering like it was done in the experiments with lysozyme above. Indeed, the 1440

$\text{cm}^{-1}$  band assigned to deformation of acyl side-chains (bending vibrations of methyl and methylene groups)<sup>38</sup> gets more prominent with time (right panel of Figure 5). Though it may be indicative, the present Raman spectra, however, do not provide sufficient evidence to reach more specific conclusions.

As evidenced by the results presented in Figure 5 (left panel, the last spectrum at the top, and the right panels), the intensities of most of the bands start to decline by the later stages of the process. (In fact, the top spectrum, such as that in Figure 5 (left panel), was the last to be observed in all LTRS experiments until, suddenly, within a few seconds, the cell bursts and disappears as a refractive body.) The decrease may indicate either the completion of the virions' assembly, the initial loss of cellular material, or both. The beginning loss of intracellular material would contradict the conclusion of Grunling and coauthors<sup>23</sup> that the CM maintains its integrity right up to the moment of complete membrane collapse. Since the detailed study of the process was not our goal, we did not pursue this question further. Further specifically focused LTRS studies might help in resolving this question as well as many others concerning the saltatory nature of cell lysis by bacteriophage which still remain unanswered. The most important of them is how so small amounts of holin molecules, only 1 molecule per 1600 molecules of PG/PL of CM (see Table 2 for the amount of lipids), can bring about such a drastic disruption of the membrane that an active tetrameric  $\beta$ -Gal-R lysin complex greater than 480 kDa in mass gets full access to the murein layer of the outer membrane.<sup>24</sup>

## CONCLUSIONS

The main goal of this paper was to test the capability of LTRS, the emerging technique in single cell research, to investigate dynamic and complex cellular processes. We showed here that LTRS proved to be an efficient and powerful technique in the real time comparative investigation of the profound structural and molecular changes in individual *E. coli* cells during their lysis by two different processes: (1) lysis from outside by egg white lysozyme and (2) lysis from within by the temperature-induced temperate bacteriophage  $\lambda$ cI857. LTRS revealed that completely different changes take place in time within these bacterial cells during the two processes. These changes may be followed simultaneously and in real time at the cellular level by observing refractive properties of the cell (its shape and surface structure changes) and at the molecular/organelle level by observing the Raman signatures of the cell.

In the case of cell lysis by lysozyme, the technique enabled for the first time at the cellular level to (i) establish that Raman spectra of bacterial cells is represented mainly by RNA-, protein-, and lipid-associated bands and that contribution of cellular DNA is negligible; (ii) observe in real time the interaction of the enzyme with *E. coli* cells at different stages of the process; (iii) “visualize” a side effect of the process due to the presence of EDTA, partial unfolding of the ribosomes and partial disruption of the secondary structure of rRNA inside the cells prior to their rupture; (iv) correlate the process of cell wall disruption, as evidenced by the onset and development of asymmetric speckle scattering patterns, with release/escape of intracellular material (ribosomes, nucleic acids, proteins, etc.) quantified by the intensity changes of Raman signatures.

In the case of lysis by the temperature induced bacteriophage, Raman spectra changes observed are consistent with the results of bacteriophage production (synthesis and assembly of  $\lambda$  virions) in population-based experiments under the same conditions and suggest a possible synthesis of HSPs at an earlier stage of the process. The sensitivity of the Raman equipment used (estimated to be around 3% of the total cell protein) did not allow for measuring the contribution (to protein-related Raman signatures) of holin molecules which are also synthesized during the process. The two lysis processes also differed in the final outcome as revealed by the results of the dynamic laser light scattering experiments. In contrast to lysis by phage, complete cell destruction did not occur during lysis by lysozyme.

The results presented here open new venues for LTRS research and strongly suggest that LTRS has a great potential

especially in the investigation of real-time processes. With further expansion of the LTRS database, it may become the method of choice for the real-time, single cell research.

#### **ACKNOWLEDGMENT**

This work was supported by the Department of the Army, through Contract W81XWH-07-2-0027.

#### **SUPPORTING INFORMATION AVAILABLE**

Additional information as noted in text. This material is available free of charge via the Internet at <http://pubs.acs.org>.

Received for review May 20, 2008. Accepted January 28, 2009.

AC8023476